Coulomb and nuclear potentials between deformed nuclei

L. C. Chamon, G. P. A. Nobre, D. Pereira, E. S. Rossi, Jr., and C. P. Silva
Departamento de Física Nuclear, Instituto de Física da Universidade de São Paulo, Caixa Postal 66318, 05315-970, São Paulo, SP, Brazil

L. R. Gasques
Department of Physics and The Joint Institute for Nuclear Astrophysics, University of Notre Dame, Notre Dame, Indiana 46556, USA

B. V. Carlson
Departamento de Física, Instituto Technológico de Aeronáutica, Centro Técnico Aeroespacial, São José dos Campos, SP, Brazil
(Received 23 March 2004; published 12 July 2004)

We present a systematics for the octupole and quadrupole deformation parameters of heavy nuclei. We also provide useful procedures to calculate the Coulomb and nuclear potentials for systems involving deformed nuclei.

DOI: 10.1103/PhysRevC.70.014604 PACS number(s): 24.10.Ht, 21.10.Ft, 21.10.Ky

I. INTRODUCTION

The forces between extended objects is a very important subject in heavy-ion collisions, where the double-folding potential plays a fundamental role in the description of the corresponding interaction. The folding of two spherically symmetric distributions can easily be calculated by using the Fourier transform representation [1]. However, when dealing with deformed distributions the obtainment of the potential is a hard task due to the numerical resolution of the corresponding six-dimensional integral, which is very time-consuming. This problem is quite relevant because most nuclei present permanent and/or vibrational deformations. Several articles have presented approximate expressions for the corresponding Coulomb interaction (e.g., Refs. [2,3]), but in general those expressions were obtained assuming only one deformed nucleus and sometimes also assuming vanishing diffuseness for the distribution. The nuclear potential has also been obtained (e.g. Ref. [4]), but again in an approximate form.

In the present paper, we provide a model to obtain approximate expressions for the Coulomb potential between two deformed nuclei with finite diffuseness. The corresponding results are compared with those obtained from the resolution of the six-dimensional integral. We also indicate a way to calculate the nuclear potential accurately, based on a zero-range model recently proposed [5]. Furthermore, we present an interesting systematics for the quadrupole and octupole deformation parameters of heavy-nuclei.

II. QUADRUPOLE AND OCTUPOLE DEFORMATION SYSTEMATICS

In an earlier paper [5], we presented an extensive systematics for the densities of heavy nuclei, based on studies of experimental charge distributions and theoretical densities calculated through the Dirac-Hartree-Bogoliubov model. In that work, we adopted a spherically symmetric two-parameter Fermi (2pF) distribution to describe the nuclear densities. We found that the radii of the charge distributions can be well described by

$$R_c = 1.76Z^{1/3} - 0.96 \text{ fm}, \tag{1}$$

where Z is the number of protons of the nucleus. The charge densities present an average diffuseness value of $a = 0.53$ fm. Owing to specific nuclear structure effects (single particle and/or collective), the parameters R_c and a show small variations around the corresponding average values throughout the Periodic Table.

In the present paper, with the aim of obtaining the deformation parameters, we have used the systematics for the quadrupole $B(E2)$ and octupole $B(E3)$ transition probabilities of even-even nuclei from Refs. [6,7]. We define the corresponding deformation lengths by $\delta_2 = \beta_2 R_c$ and $\delta_3 = \beta_3 R_c$, and we assume the following connection with the transition probabilities:

$$B(E\lambda) = \left(\frac{3Ze\beta_\lambda R_c^\lambda}{4\pi} \right)^2. \tag{2}$$

Figure 1 and 2 present the extracted values for the deformation lengths as a function of the number of protons or neutrons of the nuclei. Strong effects of structure are observed for the δ_2 parameter, which presents local minimum values at the magic numbers. With the purpose of emphasizing this behavior, we have calculated average values over isotopes and also over isotones (Fig. 3). Similar procedure has also been applied to the δ_3 parameter (Fig. 4). Most $B(E2)$ and $B(E3)$ values have been obtained through methods that involve mainly the electromagnetic interaction, such as Coulomb excitation, electron scattering, etc. Thus, one could expect that the extracted deformation lengths should be related mainly with the number of protons of the nuclei. However, an inspection of Figs. 1–4 shows a very interesting similarity between the behavior of the deformation parameters as a function of Z and N. Based on these findings, we propose that the deformation lengths can approximately be described using the following functions:

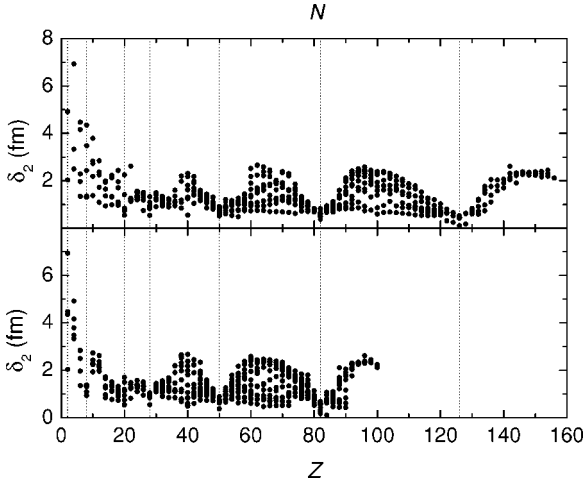

FIG. 1. The values of the quadrupole deformation lengths as a function of the number of protons (bottom) or neutrons (top) of the nuclei. The dotted lines represent the magic numbers.

$$\delta_2 = D_2(Z) + D_2(N), \tag{3}$$

$$\delta_3 = D_3(Z) + D_3(N), \tag{4}$$

where $D_3(X) = \alpha/\sqrt{X}$ with $\alpha = 3.2$ fm, and the function $D_2(X)$ is given in Table I. Expressions (3) and (4) describe the complete set of experimentally extracted deformation lengths with a dispersion (standard deviation) of 0.2 fm (about 15% precision). This precision is only slightly greater than the experimental uncertainties.

A comparison between functions D_2 and D_3 is shown in Fig. 5. The effects of shell structure observed in D_2 but not in D_3 are well understood microscopically. To lowest order, collective quadrupole transitions are constructed of a linear combination of $J=2$, positive parity particle-hole excitations. Within open shells, such excitations involve states within the same major shell. At shell closures, however, the particle state must be one from two major shells above the closed

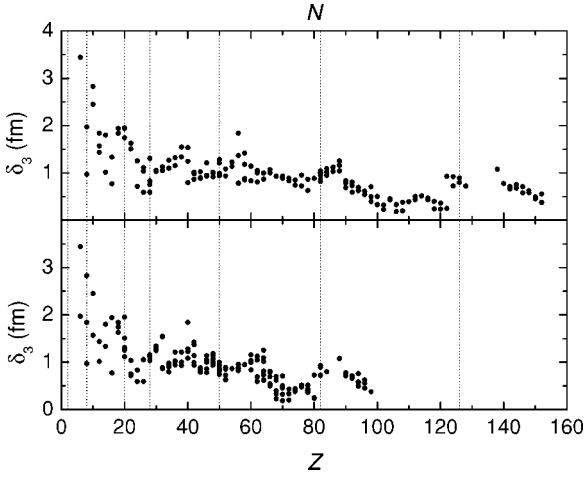

FIG. 2. The values of the octupole deformation lengths as a function of the number of protons (bottom) or neutrons (top) of the nuclei. The dotted lines represent the magic numbers.

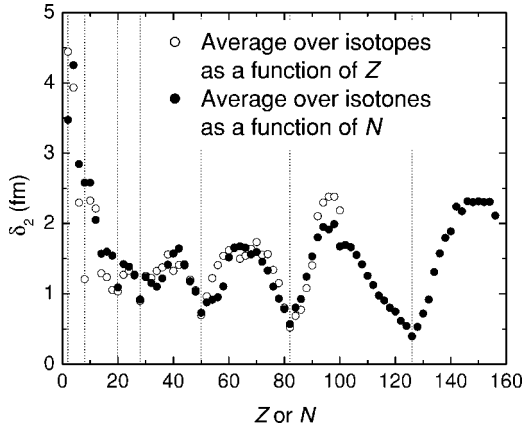

FIG. 3. The average values for isotopes (or isotones) of the quadrupole deformation lengths as a function of the number of protons (or neutrons) of the nuclei.

shell, which inhibits the excitation due to the large energy involved. D_2 is thus large where a shell is filling and tend to zero at its closure. Collective octupole transitions, on the other hand, are a linear combination of $J=3$, negative parity particle-hole excitations, which involve a hole state from one shell and a particle state from the adjacent shell. Since such combinations always exist, independently of shell closures, little structure is observed in D_3.

In the next sections we deal with deformed densities assuming the 2pF shape:

$$\rho(\vec{r}) = \frac{\rho_0}{1 + \exp\left(\dfrac{r - R(\theta_0)}{a}\right)}, \tag{5}$$

$$R(\theta_0) = R_0 + \sum \delta_\lambda Y_{\lambda 0}(\theta_0), \tag{6}$$

where θ_0 is the angle between $\mathbf{r}$ and the symmetry axis of the deformation. For the charge distributions we assume that R_0 can be described by Eq. (1), and we limit our study only to

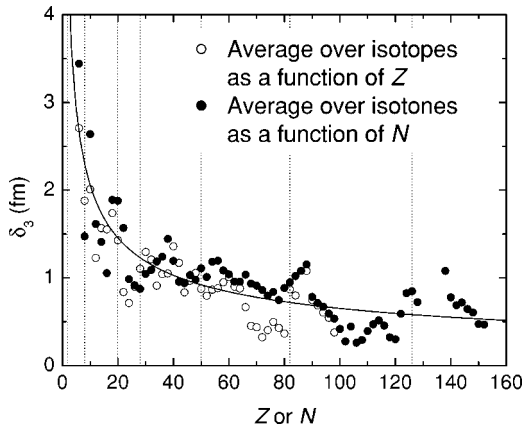

FIG. 4. The average values for isotopes (or isotones) of the octupole deformation lengths as a function of the number of protons (or neutrons) of the nuclei. The solid line represents a function proportional to $X^{-1/2}$, where X could be Z or N.

TABLE I. Values of the function $D_2(X)$.

X	D_2 (fm)	X	D_2 (fm)	X	D_2 (fm)	X	D_2 (fm)
2	2.61	42	0.75	82	0.00	122	0.54
4	2.30	44	0.67	84	0.02	124	0.51
6	0.98	46	0.43	86	0.11	126	0.08
8	0.37	48	0.30	88	0.39	128	0.23
10	1.36	50	0.00	90	0.73	130	0.59
12	1.18	52	0.28	92	1.06	132	0.68
14	0.57	54	0.62	94	1.21	134	0.87
16	0.65	56	0.77	96	1.27	136	0.99
18	0.54	58	0.83	98	1.34	138	1.05
20	0.27	60	0.95	100	1.13	140	1.17
22	0.64	62	0.93	102	1.18	142	1.31
24	0.78	64	0.99	104	1.18	144	1.06
26	0.64	66	1.10	106	1.21	146	1.07
28	0.30	68	0.99	108	1.09	148	1.10
30	0.60	70	0.91	110	1.01	150	1.10
32	0.60	72	0.80	112	0.82	152	1.05
34	0.81	74	0.63	114	0.84	154	1.06
36	0.70	76	0.43	116	0.64	156	0.98
38	0.67	78	0.26	118	0.63	158	
40	0.70	80	0.00	120	0.59	160	

quadrupole and octupole deformations. We refer as the corresponding non deformed density to

$$\rho^{(0)}(r) = \frac{\rho_0^{(0)}}{1 + \exp\left(\frac{r - R_0}{a}\right)}. \tag{7}$$

Due to the normalization condition, as defined by Eq. (8), one should observe that $\rho_0 \neq \rho_0^{(0)}$,

$$\int \rho(\mathbf{r}) d\mathbf{r} = Z. \tag{8}$$

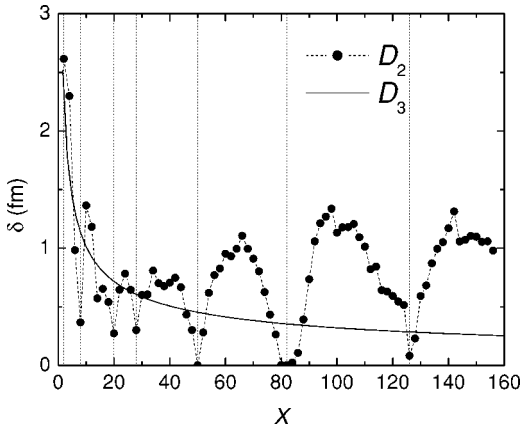

FIG. 5. The functions D_2 and D_3 that describe the behavior of the deformation lengths. The dotted lines represent the magic numbers.

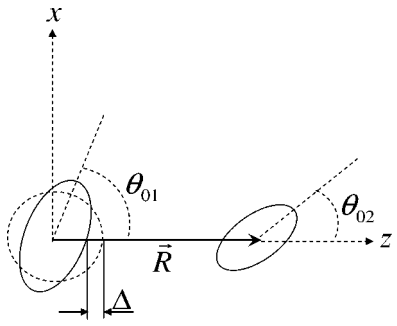

FIG. 6. Schematic picture of the collision of two deformed nuclei. The dashed circle represents the nucleus 1 if it did not have deformation.

III. THE COULOMB POTENTIAL

The Coulomb interaction between two charge distributions is given by

$$V_C(R) = \int\int \frac{e^2}{|\mathbf{R} + \mathbf{r}_2 - \mathbf{r}_1|} \rho_1(\mathbf{r}_1)\rho_2(\mathbf{r}_2) d\mathbf{r}_1 d\mathbf{r}_2, \tag{9}$$

where $\mathbf{R}$ is the position vector of the center of mass of nucleus 2 measured from that of the nucleus 1 (see Fig. 6), and describes their relative motion. We assume a system of coordinates with the z axis in the direction of $\mathbf{R}$ and the x axis in the way that the plane xz contains the symmetry axis of the deformation of nucleus 1. Therefore the direction of this symmetry axis is defined just by the angle θ_{01}. The direction of the symmetry axis of the deformation of nucleus 2 is defined by two angles: θ_{02} and the azimuthal angle ϕ_{02} (for convenience, we choose $\phi_{02}=0$ in Fig. 6).

For spherically symmetric densities, the Fourier transform representation applied to Eq. (9) results in

$$V_C^{(0)}(R) = \frac{2Z_1Z_2e^2}{\pi} \int_0^\infty J_0(qR)\hat{\rho}_1(q)\hat{\rho}_2(q) dq, \tag{10}$$

$$\hat{\rho}(q) = \frac{4\pi}{Z} \int_0^\infty J_0(qr) r^2 \rho^{(0)}(r) dr. \tag{11}$$

Furthermore, in the case of vanishing diffuseness ($a=0$) one obtains

$$V_C^{(0)}(R) = \frac{18Z_1Z_2e^2}{\pi} \int_0^\infty J_0(qR) \frac{J_1(qR_{01})}{qR_{01}} \frac{J_1(qR_{02})}{qR_{02}} dq. \tag{12}$$

Figure 7 presents a comparison of the results for $V_C^{(0)}$ obtained by (i) Eq. (10) (using the average diffuseness of Ref. [5]: $a=0.53$ fm) (ii) Eq. (12), i.e., $a=0$, (iii) Eq. (13) of the pointlike model, and (iv) Eq. (14) of the pointlike plus uniform charge model, which can often be found in textbooks on heavy-ion collisions. The different models provide very similar results in the region of the barrier radius and, therefore, such models give similar scattering cross sections except, perhaps, at high bombarding energies where the internal region of the interaction may be probed,

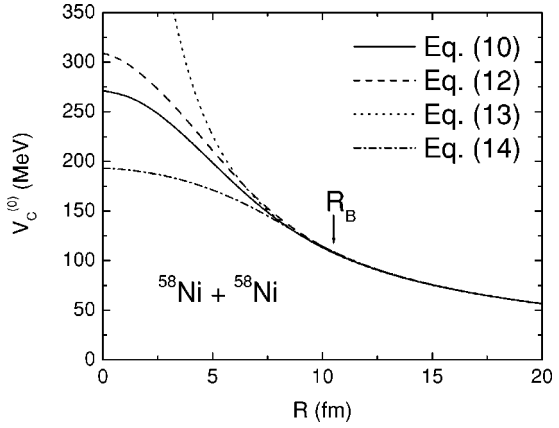

FIG. 7. The Coulomb potential calculated through different models for the ^{58}Ni+^{58}Ni system. The arrow represents the approximate position of the corresponding s-wave barrier radius.

$$V_C^{(0)}(R) = \frac{Z_1 Z_2 e^2}{R}, \tag{13}$$

$$V_C^{(0)}(R) = Z_1 Z_2 e^2 \begin{cases} 1/R & (R > R_C = R_{01} + R_{02}) \\ \dfrac{1}{2R_C}\left[3 - \dfrac{R^2}{R_C^2}\right] & (R < R_C). \end{cases} \tag{14}$$

For deformed densities, the computational resolution of Eq. (9) is very time-consuming due to the six-dimensional integral. This becomes a problem in studies where it should be solved several times as, for example, in calculations of sub-barrier fusion where the cross sections are obtained as an average over different orientations of the deformation axes. Therefore, faster methods to obtain good approximations for the deformed potential are quite convenient. In Ref. [3] was studied the interaction between a deformed projectile and a spherically symmetric target, considering both distributions with $a=0$ (the way to extend the results to finite diffuseness was indicated in that paper). We use those results as a starting point to present more general expressions.

We divide the Coulomb potential in two contributions: $V_C(R)=V_C^{(0)}(R)+V_C^{\mathrm{Cor}}(R)$, where $V_C^{(0)}(R)$ is obtained through Eq. (10) using the corresponding nondeformed densities. We have solved Eq. (9) using a Monte Carlo method and, therefore, the corresponding results have statistical uncertainties. In our studies, we have assumed the ^{58}Ni+^{58}Ni system as an example. The deformation parameters of ^{58}Ni are $\beta_2=0.205$ fm and $\beta_3=0.235$ fm, but in some simulations these values have been changed, including simulations where the two nuclei were considered with different deformations. In Fig. 8, we show that V_C^{Cor} is a relatively small correction of $V_C^{(0)}$ (about 3%), and therefore the statistical uncertainty in the calculation of V_C, through Eq. (9), must be very small to provide useful results for V_C^{Cor}. However, besides relatively small, the correction is quite important because it can reach about 4 MeV at the region of the barrier radius (see Fig. 8) and this certainly produces great effects on, for instance, fusion cross sections.

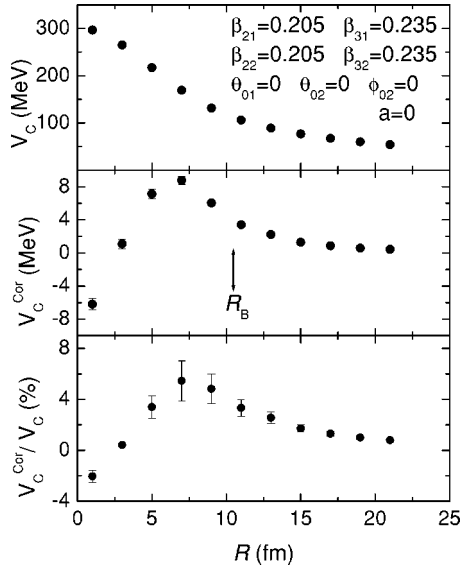

FIG. 8. The figure presents the total Coulomb potential (V_C), the correction (V_C^{Cor}) and the corresponding relative values ($100\ V_C^{\mathrm{Cor}}/V_C$) for the ^{58}Ni+^{58}Ni system. The arrow indicates the approximate position of the barrier radius.

According to Ref. [3], as long as only nucleus 1 is deformed, the symmetry axes of the deformations are in the same direction, and the diffuseness of the distributions is $a=0$, the correction of the Coulomb potential can be approximately described by the following set of equations:

$$V_C^{\mathrm{Cor}}(R) = V^{(1)}(R) + V^{(2)}(R), \tag{15}$$

$$V^{(1)}(R) = Z_1 Z_2 e^2 [\beta_{21} F_2^{(1)}(R;R_{01};R_{02}) Y_{20}(\theta_{01}) + \beta_{31} F_3^{(1)}(R;R_{01};R_{02}) Y_{30}(\theta_{01})], \tag{16}$$

$$V^{(2)}(R) = \frac{Z_1 Z_2 e^2}{\sqrt{\pi}} [\beta_{21}^2 G_2(R;R_{01};R_{02};\theta_{01}) + \beta_{31}^2 G_3(R;R_{01};R_{02};\theta_{01}) + \beta_{21}\beta_{31} G_{23}(R;R_{01};R_{02};\theta_{01})], \tag{17}$$

$$G_2(R;X;Y;\theta) = \sqrt{\frac{5}{49}} F_2^{(2)}(R;X;Y) Y_{20}(\theta) + \frac{3}{7} F_4^{(2)}(R;X;Y) Y_{40}(\theta), \tag{18}$$

$$G_3(R;X;Y;\theta) = \sqrt{\frac{4}{45}} F_2^{(2)}(R;X;Y) Y_{20}(\theta) + \frac{3}{11} F_4^{(2)}(R;X;Y) Y_{40}(\theta) + \sqrt{\frac{2500}{14157}} F_6^{(2)}(R;X;Y) Y_{60}(\theta), \tag{19}$$

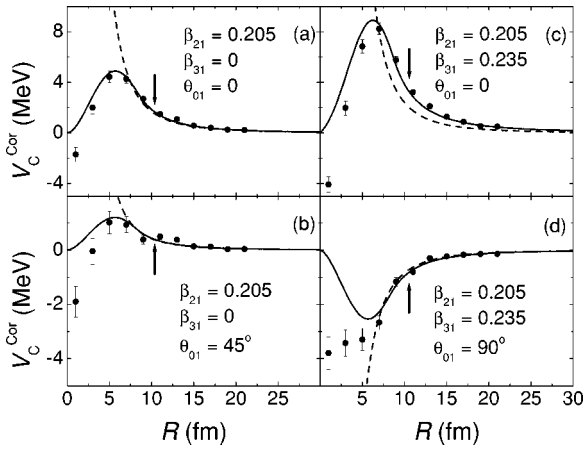

FIG. 9. The figure presents the correction of the Coulomb potential for the ^{58}Ni+^{58}Ni system. The nucleus 2 is assumed undeformed and the diffuseness of both distributions is $a=0$. The deformation parameters of nucleus 1 are indicated in the figure. The solid lines represent the results of Eqs. (15)–(22), and the dashed lines represent the asymptotic expression (23). The arrows indicate the approximate position of the barrier radius.

$$G_{23}(R;X;Y;\theta) = \sqrt{\frac{27}{35}}F_1^{(2)}(R;X;Y)Y_{10}(\theta) + \sqrt{\frac{16}{45}}F_3^{(2)}(R;X;Y)Y_{30}(\theta) + \sqrt{\frac{500}{693}}F_5^{(2)}(R;X;Y)Y_{50}(\theta), \quad (20)$$

$$F_\lambda^{(1)}(R;X;Y) = \frac{18}{\pi}\int_0^\infty J_\lambda(qR)\frac{J_1(qY)}{qY}J_\lambda(qX)dq, \quad (21)$$

$$F_\lambda^{(2)}(R;X;Y) = \frac{18}{\pi}\int_0^\infty J_\lambda(qR)\frac{J_1(qY)}{qY}\left[J_\lambda(qX) + \frac{qX}{2}\frac{dJ_\lambda(qX)}{d(qX)}\right]dq. \quad (22)$$

From this set of equations and neglecting second order terms, one can find the following asymptotic expression:

$$V_C^{\mathrm{Cor}}(R\to\infty) = Z_1Z_2e^2\left[\frac{3\beta_{21}R_{01}^2}{5R^3}Y_{20}(\theta_{01}) + \frac{3\beta_{31}R_{01}^3}{7R^4}Y_{30}(\theta_{01})\right]. \quad (23)$$

This expression (or similar) has been used in many works (e.g. Ref. [8]).

The solid lines in Fig. 9 represent the results of Eqs. (15)–(22) and the dashed ones correspond to Eq. (23). Equation (15)–(22) provide very good results, except at very inner distances. One should observe that the asymptotic expression is not accurate under certain conditions. Indeed, in the case of Fig. 9(c), for example, the second order terms are not negligible at all.

We have generalized the model for two deformed nuclei, and considering different orientations $(\theta_{\lambda i},\phi_{\lambda i})$, for each deformation of each nucleus. The corresponding correction (V_C^{Cor}) can be described by the following modifications for $V^{(1)}$ and $V^{(2)}$:

$$V^{(1)}(R) = Z_1Z_2e^2[\beta_{21}F_2^{(1)}(R;R_{01};R_{02})Y_{20}(\theta_{21}) + \beta_{31}F_3^{(1)}(R;R_{01};R_{02})Y_{30}(\theta_{31}) + \beta_{22}F_2^{(1)}(R;R_{02};R_{01})Y_{20}(\theta_{22}) - \beta_{32}F_3^{(1)}(R;R_{02};R_{01})Y_{30}(\theta_{32})], \quad (24)$$

$$V^{(2)}(R) = Z_1Z_2e^2\left\{\sum_{\substack{\lambda\neq 0\\ \lambda_a\lambda_b}}(2\lambda+1)\begin{pmatrix}\lambda_a & \lambda_b & \lambda\\ 0 & 0 & 0\end{pmatrix} \times[F_\lambda^{(2)}(R;R_{01};R_{02})\beta_{\lambda_a 1}\beta_{\lambda_b 1} \times H_{\lambda\lambda_a\lambda_b}(\theta_{\lambda_a 1},\phi_{\lambda_a 1};\theta_{\lambda_b 1},\phi_{\lambda_b 1}) + (-1)^\lambda F_\lambda^{(2)}(R;R_{02};R_{01})\beta_{\lambda_a 2}\beta_{\lambda_b 2} \times H_{\lambda\lambda_a\lambda_b}(\theta_{\lambda_a 2},\phi_{\lambda_a 2};\theta_{\lambda_b 2},\phi_{\lambda_b 2}) + i^{\lambda+\lambda_b-\lambda_a}F_{\lambda\lambda_a\lambda_b}^{(3)}(R;R_{01};R_{02})\beta_{\lambda_a 1}\beta_{\lambda_b 2} \times H_{\lambda\lambda_a\lambda_b}(\theta_{\lambda_a 1},\phi_{\lambda_a 1};\theta_{\lambda_b 2},\phi_{\lambda_b 2})]\right\}, \quad (25)$$

$$F_{\lambda\lambda_a\lambda_b}^{(3)}(R;X;Y) = \frac{18}{\pi}\int_0^\infty J_\lambda(qR)J_{\lambda_a}(qX)J_{\lambda_b}(qY)dq, \quad (26)$$

$$H_{\lambda\lambda_a\lambda_b}(\theta_1,\phi_1;\theta_2,\phi_2) = \sum_{\mu_a\mu_b}\begin{pmatrix}\lambda_a & \lambda_b & \lambda\\ \mu_a & \mu_b & 0\end{pmatrix}Y_{\lambda_a\mu_a}^*(\theta_1,\phi_1) \times Y_{\lambda_b\mu_b}^*(\theta_2,\phi_2), \quad (27)$$

where we have used the 3-j symbols [9].

Our simulations have indicated that such expressions are quite accurate (Fig. 10). Finally, to complete the generalization, we have observed (Fig. 11) that the model also works for distributions with $a\neq 0$, using the same expressions (with $a=0$) for V_C^{Cor}, but considering in the calculation of $V_C^{(0)}$, through Eqs. (10) and (11), the corresponding nondeformed densities with $a\neq 0$. This point is important because $V_C^{(0)}$ is dependent on a. In Figs. 10 and 11 one can observe, again, that the asymptotic expression (23), generalized for two deformed nuclei, fails in some cases.

IV. THE NUCLEAR POTENTIAL

We have developed a model for the nuclear interaction which is based on the effects of the Pauli nonlocality [5,10,11]. This interaction has been successful in describing the elastic scattering, peripheral reaction channels, and fusion involving heavy-ion systems [12–20]. Within the nonlocal model, the nuclear interaction V_N is connected with the folding potential V_F through [5]

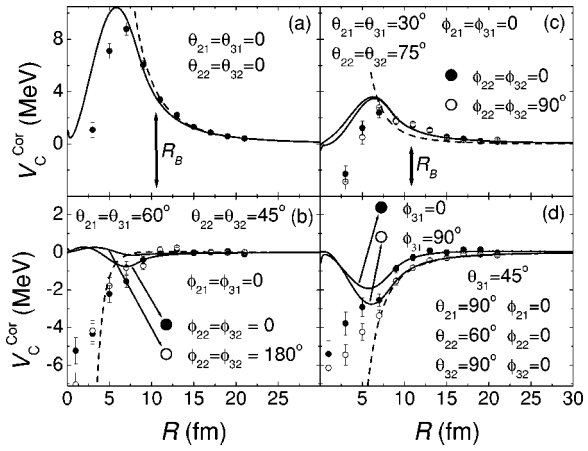

FIG. 10. The figure presents the correction of the Coulomb potential for the ^{58}Ni+^{58}Ni system, where $\beta_2=0.205$, $\beta_3=0.235$, and $a=0$ were assumed for both nuclei. The angles of the deformation axes are indicated in the figure. The arrows indicate the approximate position of the barrier radius.

$$V_N(R) = V_F(R)e^{-4v^2/c^2}, \tag{28}$$

where c is the speed of light and v is the local relative velocity between the two nuclei. In the present paper, we only study the folding potential [Eq. (29)] because the corresponding nuclear interaction can be obtained through it by considering the term involving the relative velocity,

$$V_F(R) = \int \rho_{N1}(\mathbf{r}_1)\rho_{N2}(\mathbf{r}_2)v_{NN}(\mathbf{R}-\mathbf{r}_1+\mathbf{r}_2)d\mathbf{r}_1 d\mathbf{r}_2. \tag{29}$$

Usually, in Eq. (29) ρ_{Ni} are the nucleon densities of the nuclei, and v_{NN} is the effective nucleon-nucleon interaction. In many works, the Paris and Reid versions of the M3Y interaction [1] have been assumed for $v_{NN}(r)$. In Ref. [5], we have demonstrated that the folding type interaction, Eq. (30), produces very similar results in comparison with those from the M3Y:

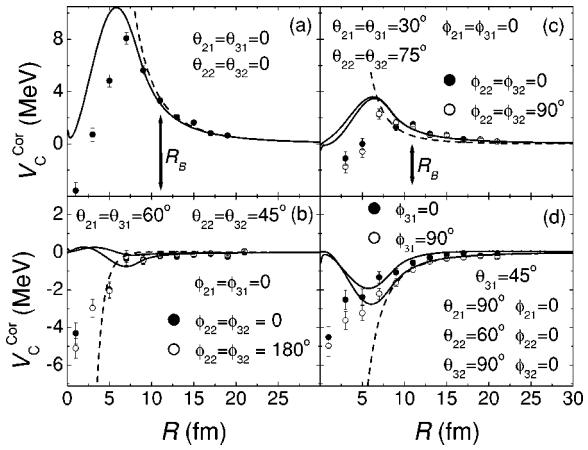

FIG. 11. The same as Fig. 10, but for $a=0.53$ fm.

$$v_{NN}(r) = \int \rho_m(r_1)\rho_m(r_2)V_0\delta(\mathbf{r}-\mathbf{r}_1+\mathbf{r}_2)d\mathbf{r}_1 d\mathbf{r}_2, \tag{30}$$

where $V_0=-456$ MeV fm^3 and ρ_m is the matter density of the nucleon. Based on the intrinsic charge distribution of the proton in free space, which has been determined by electron scattering experiments, an exponential shape has been assumed for the matter density of the nucleon [5]. Due to the delta function, the folding in Eq. (30) is named as the zero-range approach. We have also defined [5] the matter density of the nucleus by folding the corresponding nucleon density with the matter density of the nucleon

$$\rho_M(\mathbf{r}) = \int \rho_N(\mathbf{r}')\rho_m(\mathbf{r}-\mathbf{r}')d\mathbf{r}'. \tag{31}$$

Thus, we distinguish the matter density of the nucleus from the nucleon one by taking into account the finite size of the nucleon. By inserting Eqs. (30) and (31) in Eq. (29), the folding potential can be recast in the following form:

$$V_F(R) = \int \rho_{M1}(\mathbf{r}_1)\rho_{M2}(\mathbf{r}_2)V_0\delta(\mathbf{R}-\mathbf{r}_1+\mathbf{r}_2)d\mathbf{r}_1 d\mathbf{r}_2$$

$$= V_0 \int \rho_{M1}(\mathbf{r}_1)\rho_{M2}(\mathbf{r}_1-\mathbf{R})d\mathbf{r}_1. \tag{32}$$

In Ref. [5], we provided a systematics also for the nucleon and matter densities. The radii of both distributions are well described by

$$R_0 = 1.31A^{1/3} - 0.84 \text{ fm}. \tag{33}$$

Due to the folding procedure, the average diffuseness for the matter densities, $a_M=0.56$ fm, is slightly greater than that for the nucleon distributions, $a_N=0.50$ fm.

Due to the six-dimensional integral, the numerical resolution of Eq. (29) implies a similar problem as that for the Coulomb potential. Equation (32) is much easier to solve because the zero-range approach reduces it to a three-dimensional integral. We have calculated the folding potential, through Eq. (32), for the ^{58}Ni+^{58}Ni (solid lines in Fig. 12). With the purpose of comparison, the dashed lines in Fig. 12 represent the nondeformed folding potential ($V_F^{(0)}$), which has been calculated considering the corresponding nondeformed densities. At the surface, the deformed potential can differ by a factor about 4 in comparison with the nondeformed one.

For large distances, the nondeformed potential has an approximate exponential shape

$$V_F^0(R) \approx U_0 e^{-(R-R_{01}-R_{02})/a_P}, \tag{34}$$

where the index P has been used to differ the diffuseness of the potential from that of the density. Taking into account that $V_F^{(0)}$ depends mostly on the distance between the surfaces of the nuclei ($s=R-R_{01}-R_{02}$), approximate expressions have been proposed to describe the deformed potential. For instance, Eqs. (35) and (36) depend on the variation of the radii of the densities along the z axis (Fig. 6 shows Δ only for nucleus 1)

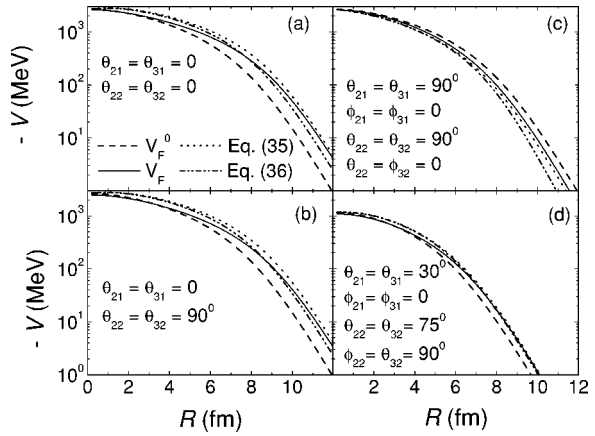

FIG. 12. The deformed nuclear potential (solid lines) compared with the nondeformed one (dashed lines) for the ^{58}Ni+^{58}Ni system. The figure also presents the results obtained with the usual approximations, Eqs. (35) and (36). $\beta_2=0.205$, $\beta_3=0.235$, and $a_M=0.56$ fm were assumed for both nuclei. The angles of the deformation axes are indicated in the figure.

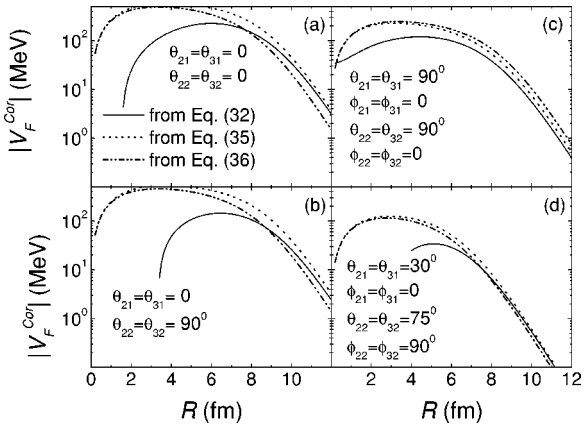

FIG. 13. The absolute value for the correction $V_F^{\rm Cor}=V_F-V_F^{(0)}$, where the folding potential was obtained from Eqs. (32), (35), and (36). The deformation parameters are the same as those in Fig. 12.

$$V_F(R) \approx V_F^{(0)}(R)e^{\Delta/a_P}, \tag{35}$$

$$V_F(R) \approx V_F^{(0)}(R) - \Delta\frac{dV_F^{(0)}}{dR}, \tag{36}$$

where the variation of the radii is defined by

$$\Delta = \delta_{21}Y_{20}(\theta_{21}) + \delta_{31}Y_{30}(\theta_{31}) + \delta_{22}Y_{20}(\theta_{22}) - \delta_{32}Y_{30}(\theta_{32}). \tag{37}$$

Taking into account the approximate exponential shape of the potential, the diffuseness involved in Eq. (35) can be estimated from

$$a_P = -V_F^{(0)}(R)\left[\frac{dV_F^{(0)}}{dR}\right]^{-1}. \tag{38}$$

Figure 12 shows the results for the deformed and nondeformed folding potentials and also those from Eqs. (35) and (36). In Fig. 13, we show the corresponding corrections $V_F^{\rm Cor}=V_F-V_F^{(0)}$. Equation (35) provides better approximations than Eq. (36). Even so, in the surface region the correction from Eq. (35) may differ by about 40% from the more accurate results obtained with Eq. (32).

V. CONCLUSION

Our systematics for the deformation lengths shows very interesting features: (i) the symmetry between the contributions of neutrons and protons, and (ii) the contrast between the strong structure effects on δ_2 compared with the smoothness of δ_3. The systematics has been performed with basis on experimental results for stable even-even nuclei, and our analysis indicates that it can be used to estimate deformation parameters within about 15% precision. A test of the predictions for other sort of nuclei, such as the exotic ones, would be very interesting.

We have provided a model to calculate the Coulomb potential between two deformed nuclei with finite diffuseness. Our model produces precise estimations in the surface region, where the usual asymptotic expressions fail in certain cases. A reasonable estimation of the deformed Coulomb interaction is also obtained in the inner region. The way proposed to calculate the nuclear potential, which is based on the zero-range approach, makes the numerical calculation much faster than that using the finite-range effective nucleon-nucleon interaction. We have demonstrated that the usual approximations may significantly differ from the more accurate results.

The findings of the present work should be useful in studies of heavy-ion reactions, particularly for the sub-barrier fusion process where the deformations of the nuclei play an important role.

ACKNOWLEDGMENTS

This work was partially supported by Financiadora de Estudos e Projetos (FINEP), Fundação de Amparo à Pesquisa do Estado de São Paulo (FAPESP), Conselho Nacional de Desenvolvimento Científico e Tecnológico (CNPq), and The Joint Institute for Nuclear Astrophysics (JINA) NSF PHY 0216783.

[1] G. R. Satchler and W. G. Love, Phys. Rep. **55**, 183 (1979).
[2] H. J. Krappe, Ann. Phys. (N.Y.) **99**, 142 (1976).
[3] N. Takigawa, T. Rumin, and N. Ihara, Phys. Rev. C **61**, 044607 (2000).
[4] M. Ismail, A. Y. Ellithi, and F. Salah, Phys. Rev. C **66**, 017601 (2002).
[5] L. C. Chamon, B. V. Carlson, L. R. Gasques, D. Pereira, C. De Conti, M. A. G. Alvarez, M. S. Hussein, M. A. Candido

Ribeiro, E. S. Rossi, Jr., and C. P. Silva, Phys. Rev. C **66**, 014610 (2002).
[6] S. Raman, C. W. Nestor, Jr., and P. Tikkanen, At. Data Nucl. Data Tables **78**, 1 (2001).
[7] T. Kibedi and R. H. Spear, At. Data Nucl. Data Tables **80**, 35 (2002).
[8] H. Esbensen, Nucl. Phys. **A352**, 147 (1981).
[9] A. R. Edmonds, *Angular Momentum in Quantum Mechanics* (Princeton University Press, Princeton, NJ, 1960).
[10] L. C. Chamon, D. Pereira, M. S. Hussein, M. A. Candido Ribeiro, and D. Galetti, Phys. Rev. Lett. **79**, 5218 (1997).
[11] M. A. Candido Ribeiro, L. C. Chamon, D. Pereira, M. S. Hussein, and D. Galetti, Phys. Rev. Lett. **78**, 3270 (1997).
[12] L. C. Chamon, D. Pereira, and M. S. Hussein, Phys. Rev. C **58**, 576 (1998).
[13] L. R. Gasques, L. C. Chamon, C. P. Silva, D. Pereira, M. A. G. Alvarez, E. S. Rossi, Jr., V. P. Likhachev, B. V. Carlson, and C. De Conti, Phys. Rev. C **65**, 044314 (2002).
[14] M. A. G. Alvarez *et al.*, Phys. Rev. C **65**, 014602 (2002).
[15] E. S. Rossi, Jr., D. Pereira, L. C. Chamon, C. P. Silva, M. A. G. Alvarez, L. R. Gasques, J. Lubian, B. V. Carlson, and C. De Conti, Nucl. Phys. **A707**, 325 (2002).
[16] T. Tarutina, L. C. Chamon, and M. S. Hussein, Phys. Rev. C **67**, 044605 (2003).
[17] L. R. Gasques, L. C. Chamon, D. Pereira, M. A. G. Alvarez, E. S. Rossi, Jr., C. P. Silva, G. P. A. Nobre, and B. V. Carlson, Phys. Rev. C **67**, 067603 (2003).
[18] L. R. Gasques *et al.*, Phys. Rev. C **67**, 024602 (2003).
[19] M. A. G. Alvarez, L. C. Chamon, M. S. Hussein, D. Pereira, L. R. Gasques, E. S. Rossi, Jr., and C. P. Silva, Nucl. Phys. **A723**, 93 (2003).
[20] L. R. Gasques, L. C. Chamon, D. Pereira, M. A.G. Alvarez, E. S. Rossi, Jr., C. P. Silva, and B. V. Carlson, Phys. Rev. C **69**, 034603 (2004).